Batteries & Supercaps

Research Article
doi.org/10.1002/batt.202200270

Chemistry Europe
European Chemical Societies Publishing

www.batteries-supercaps.org

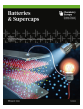

Non-Thermal Plasma Assisted Fabrication of Ultrathin $NiCoO_x$ Nanosheets for High-Performance Supercapacitor

Birhanu Bayissa Gicha,[a, b] Lemma Teshome Tufa,[c, d] Mahendra Goddati,[e] Samir Adhikari,[f] Juyoung Gwak,[e] and Jaebeom Lee*[a, e]

Transition metal based layered double hydroxides (TMLDHs) are potential candidates for supercapacitors; however, their structural staking often limits their energy density, one of the major pending obstacles in the sector. Simple, fast, and safe modification strategies such as exfoliation of jammed layers into single sheets can be a viable option to overcome those challenges. This work reports fabrication of an ultrathin nanosheets from bulk TMLDHs using superficial non-thermal Ar-plasma exfoliation strategy. Electrochemical characterizations have confirmed that capacitive performance of pristine $NiCoO_x$ nanosheets has improved because of Ar-plasma induced exfoliation. A remarkable of 5.7 $F\,cm^{-2}$ areal capacitance was achieved at a current density of 5 $mA\,cm^{-2}$ for ultrathin Ar-$NiCoO_x$ nanosheets. The material also exhibited excellent cyclic stability with over 88% capacitance retention after 5000 cycles. The electrode material assembled into symmetric supercapacitor device delivering an energy density of 85.9 $\mu Wh\,cm^{-2}$ at a power density of 500 $\mu W\,cm^{-2}$ .The higher supercapacitive performance is attributed to increased electrochemical surface area and improved capability of electron and ion transport induced by Ar-plasma exfoliation, demonstrating an opportunity for further use of TMLDHs in the energy conversion and storage sector.

Introduction

Breakthrough advancement of renewable energy-storage technologies are indispensable to curtail the severe environmental disaster stemming from ever-increasing global energy consumption.[1,2] Recently, supercapacitors (SCs) have shown remarkable potential as energy storage device due to their higher power density, short charging time, and excellent rate capability.[3–5] However, the major pending obstacle pertaining to their low energy density compared to batteries have considerably limited their commercialization in wide-scale energy storage systems.[6] Efforts are poured to enhance the energy storage performance of SCs while maintaining its higher power density through rational design of electrode materials mainly sourcing from transition metals.

As an imminent class of 2D nanomaterial, layered double hydroxides of transition metals (TMLDHs) have drained growing attention as promising electrode materials for SCs.[7–10] TMLDHs are group of anionic lamellar with brucite-like host layers generally represented as $[M_{1-x}^{2+}M_x^{3+}(OH)_2]$-$A_{x/n}^{n-}\cdot mH_2O$, where M^{2+} stands for bivalent metal cations, and M^{3+} stands for trivalent metal cations, A^{n-} is anionic interlayer.[11,12] TMLDHs are exalted for their high catalytic activity, ease of fabrication, and their low-cost sourcing from abundant sources.[13] Their unique lamellar structure endows them with flexibility of the metal cation host layers and tunable interlayer distance resulting with many fascinating electrochemical features.[14] Nevertheless, the application of TMLDHs as electrode materials for SCs is limited mainly due to its poor electrical conductivity and inaccessibility of the active sites because of its jammed layers manifested as poor cycling stability, low specific capacitance, and inferior rate capability.[15] To address these issues and expand the scope of its application, it is essential to modify jammed layers of TMLDHs to thin nanosheets, enhancing electrochemical surface area for high charge storage.

Numerous modification strategies such as exfoliation and doping have been widely employed to manipulate the structure and composition of TMLDHs to enhance their capacitive performances.[16,17] In particular, exfoliation is widely used to obtain an ultrathin nanosheet layers exposing more active sites and enhance surface area, creating abundant storage sites for the guest ions to attain higher capacitance.[18]

[a] Dr. B. B. Gicha, Prof. J. Lee
Department of Chemistry
Chungnam National University
Daejeon, 34134, Republic of Korea
E-mail: nanoleelab@cnu.ac.kr
[b] Dr. B. B. Gicha
Environmental Science Program
Haramaya University
Dire Dawa, 138, Ethiopia
[c] Dr. L. T. Tufa
Research Institute of Materials Chemistry
Chungnam National University
Daejeon, 34134, Republic of Korea
[d] Dr. L. T. Tufa
Department of Applied Chemistry
Adama Science and Technology University
P.O. Box 1888, Adama, Ethiopia
[e] M. Goddati, J. Gwak, Prof. J. Lee
Department of Chemical Engineering and Applied Chemistry
Chungnam National University
Daejeon, 34134, Republic of Korea
[f] Dr. S. Adhikari
Institute of Quantum Systems
Chungnam National University
Daejeon, 34134, Republic of Korea

Supporting information for this article is available on the WWW under https://doi.org/10.1002/batt.202200270

Research Article
doi.org/10.1002/batt.202200270
Chemistry Europe
European Chemical Societies Publishing

For instance, Quan et al.[19] employed exfoliation technique to restack Ni-Mn LDH and MnO_2 nanosheet composites with improved capacitive performances. The as-synthesized material has demonstrated higher energy density of 16 $Wh\,kg^{-1}$ at a power density of 15 $kW\,kg^{-1}$. Li and co-workers[20] were also able to exfoliate Co-Al LDH and GO (graphene oxide) into Co-Al LDH-NS/GO-NS (NS for nanosheet) with improved electrochemical performance as asymmetric supercapacitor. Nevertheless, conventional exfoliation techniques are not safe, requiring longer treatment time and toxic chemicals.[21] On the other hand, difficulty to remove solvents after exfoliation process due to the strong affinity of TMLDHs lead to blockage of active sites, degrading capacitive performance.[22] To overcome these challenges, new exfoliation approaches are desirable. In this regard, plasma-induced exfoliation is highly hailed for its efficiency, timesaving, environmentally friendly, and the final products are free of surfactants minimizing interference.[23]

Based on the above idea, we have employed a facile and safe superficial non-thermal Ar-plasma exfoliation strategy to fabricate ultrathin $NiCoO_x$ LDHs nanosheets from its counter pristine state. A remarkable areal capacitance of 5.7 $F\,cm^{-2}$ was achieved at a current density of 5 $mA\,cm^{-2}$ for ultrathin Ar-NiCoOx nanosheets. The material also exhibited excellent cyclic stability with over 88% capacitance retention after 5000 cycles. Remarkably, the results confirmed that the exfoliation process led to the modifications of morphological and electronic structure, further enhancing the capacitive performance of TMLDHs.

Results and Discussion

The ultrathin $NiCoO_x$ nanosheets were fabricated using nickel foam (NF) as a support material via electrodeposition method followed by superficial nonthermal Ar-plasma exfoliation strategy (Figure 1a). The electrodeposition was carried out from aqueous solution of salts of nickel and cobalt nitrate (6 mM) for 40 seconds involving the following electrochemical reaction:

$$x\mathrm{Ni}^{2+} + y\mathrm{Co}^{2+} + 2(x+y)\mathrm{OH}^- \rightarrow \mathrm{Ni}_x\mathrm{Co}_y(\mathrm{OH})_{2(x+y)} \quad (1)$$

Once the electrodeposition completed, the sample was subjected to nonthermal Ar-plasma (100 W) treatment for different durations (5–30 minutes). Figure 1(b–e) shows typical scanning electron microscope (SEM) images of pristine and Ar-plasma exfoliated $NiCoO_x$ nanosheets. The entire surface of NF (Figure S1a) is covered by a vertically grown interconnected nanosheets array (Figure S1b). After the surface of the $NiCoO_x$ bulk LDHs was treated with Ar-plasma (20 minutes) rippled silk like morphology with enlarged intercalated space appeared, indicating the successful exfoliation of the bulk material (Figure 1d,e). The process alters the basal plane of bulk $NiCoO_x$ nanosheets generating disordered porous nanostructures, exposing the electroactive sites.[24] Furthermore, rate of adsorption of electrolyte on to catalyst surface strongly influences its performance. The surface wettability of the samples was measured by water droplet contact angle (CA) test. As shown in Figure 1(f and g), Ar-$NiCoO_x$ nanosheets exhibited lower contact angle value of 11.250° compared to pristine $NiCoO_x$ with contact angle value measured at 56.550° showing an improved electrolyte-hydrophilic surface. The result shows that Ar-plasma treatment not only exfoliates the jammed layers to ultrathin nanosheets, but also modifies surface chemical property of the material enhancing prompt electrolyte ion infiltration and improves utilization of active sites of the LDHs nanosheets.[25] As shown in Figure S2, the structure and thickness of the nanostructures grown on the NF were affected by the ratio between Ni and Co, affecting the overall performance of the electrode materials. Transmission electron microscopy (TEM) was further employed to investigate the morphology of the electrode materials. Compared to pristine $NiCoO_x$ (Figure 2a) a typical TEM image of Ar-$NiCoO_x$ nanosheets (Figure 2b) shows a homogenous transparent feature, demonstrating ultrathin nature of the exfoliated nanosheets. Furthermore, the higher resolution (HR) TEM image insets in Figure 2(a,b) reveal no measurable lattice fringes revealing that the basic architecture of the layer didn't change considerably after exfoliation. The energy dispersive X-ray spectroscopy (EDX) recorded from TEM image (Figure 2c) confers the uniform distribution of Ni, Co, and O elements. The SEM EDX for the pristine $NiCoO_x$ also detects the incorporation of the desired elements in the composition (Figure S1c). A tapping-mode atomic force microscope (AFM) images further elucidates the exfoliation of pristine $NiCoO_x$ to ultrathin nanosheets. As shown in Figure 2(d,e) the thickness of pristine $NiCoO_x$ is decreased from ~53.7 nm to ~1.3 nm after Ar-plasma treatment for 20 minutes (Figure 2f).

The amorphous phase of the electrode material was confirmed by powder X-ray diffraction (XRD) pattern presented in Figure 3(a) for Ar-$NiCoO_x$ nanosheets. Diffraction peaks corresponding to Ni, Co or their composites were not detected and appearing peaks are mainly from NF.[26] The amorphous nature of the material reduces strain during charging-discharging process that improves the long cycling stability of the material. X-ray photoelectron spectroscopy (XPS) was used to further investigate the composition and electronic state of the electrode materials. It is evident from the results of the survey presented in the (Figure 3b–d) that Ar-$NiCoO_x$ nanosheets are composed of Ni, Co, and O elements (Figure S3). Nickel exists as Ni^{2+} in both pristine and Ar-plasma exfoliated nanosheets as can be depicted from the high resolution XPS (Figure 3b) with clear peaks located at 856.1 and 873.7 eV corresponding to Ni $2p_{3/2}$ and Ni $2p_{1/2}$, respectively.

For Co 2p XPS (Figure 3c), two distinct peaks appearing at 781.5 eV (Co $2p_{3/2}$) and 797.2 eV (Co $2p_{1/2}$) are indicators of $Co(OH)_2$.[27] However, once the pristine $NiCoO_x$ is treated with Ar-plasma, slight peak shift to lower energy in the region of Co $2p_{3/2}$ (781.2 eV) and Co $2p_{1/2}$ (797.0 eV) were prevalent, indicating the partial oxidation of Co^{2+} to Co^{3+}.[28] Meanwhile, the spectrum of O 1s region at 532.0 eV (Figure 3d) corroborates the M–OH bonding, further supporting the existence of the metals as hydroxides.[29]

The supercapacitive property of pristine ($NiCoO_x$) and Ar-plasma exfoliated (Ar-$NiCoO_x$) nanosheets were tested using

Research Article
doi.org/10.1002/batt.202200270
Chemistry Europe
European Chemical Societies Publishing

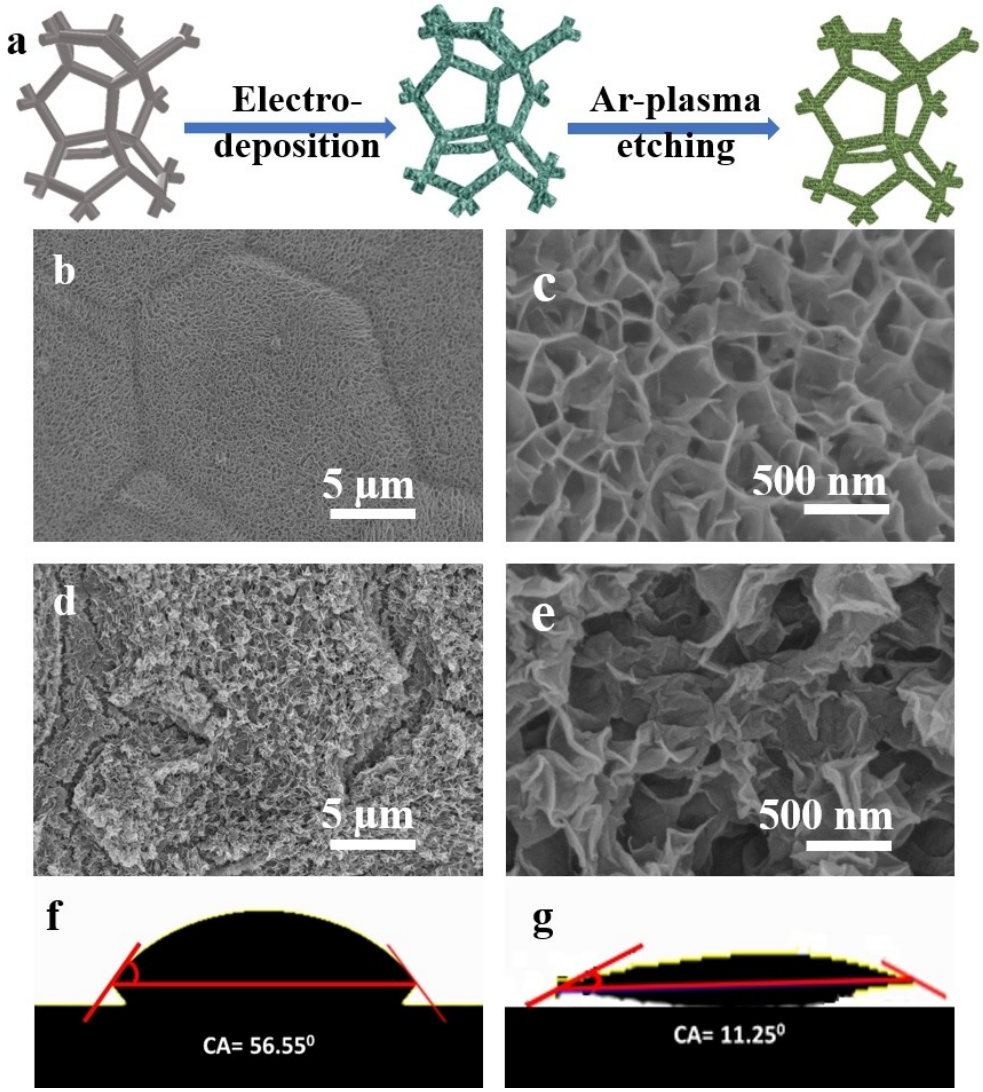

Figure 1. Schematic diagram and electron microscopic characterization of Ar-$NiCoO_x$ nanosheets. a) Illustration of the synthesis of Ar-$NiCoO_x$ nanosheets, SEM images of b) and c) NiCoOx, d) and e) Ar-NiCoOx, and contact angle for f) $NiCoO_x$, and g) Ar-NiCoO*x* nanosheets.

the sample as working electrode in a standard three-electrode system in aqueous of solution 3 M KOH. Figure 4(a) presents typical cyclic voltammetry (CV) curves of Ar-$NiCoO_x$, $NiCoO_x$, and NF substrate in the voltage range of 0.0–0.6 V at scan rate of 60 $mV\,s^{-1}$. It is apparent that the integrated area of Ar-$NiCoO_x$ nanosheets and its redox current is higher than pristine $NiCoO_x$ and NF, indicative of higher capacitance. For Ar-$NiCoO_x$ and $NiCoO_x$, pair of distinct peaks associated with the redox reactions of the metal cations appearing around 0.1 and 0.4 V are indicators of their reverse process.[30] Compared to bulk $NiCoO_x$ LDHs, Ar-$NiCoO_x$ nanosheets demonstrated a smaller oxidation-reduction energy barrier because of fast ion diffusion across the ultrathin and enlarged interlayer spacing resulting from Ar-plasma induced exfoliation of the pristine material. Compared to others, the area from CV curves of NF is negligible indicating the capacitive contribution of NF is quite small. Moreover, enhancement in the supercapacitive activity of Ar-NiCo nanosheets is confirmed from its CV response at various scan rates. Seemingly, all curves exhibit a similar shape with a pair of well-defined redox peaks, and the current density increases with increasing scan rate, which is an indicator of a good electrochemical reversibility (Figure 4b). As the scan rate increases, clearly oxidation peak shifted to the direction of positive potential and reduction peaks towards negative potential. CV curves of NF and bulk NiCo electrode materials are presented in Figure S4(a and b), respectively, for comparison. Such phenomena are associated with the surface modification of pristine NiCo with non-thermal Ar-plasma treatment enhancing the conductivity and charge transfer kinetics across ultrathin nanosheets. Like Ar-NiCo, the shapes of CV curves for NF and bulk NiCo were maintained and peak current increases with increase in sweep rates.

To further confirm the enhancement in the supercapacitive performance of the electrode material, galvanostatic charge discharge (GCD) between 0–0.5 V potential ranges was measured under a variable current density varying from 5–

Research Article
doi.org/10.1002/batt.202200270
Chemistry Europe
European Chemical Societies Publishing

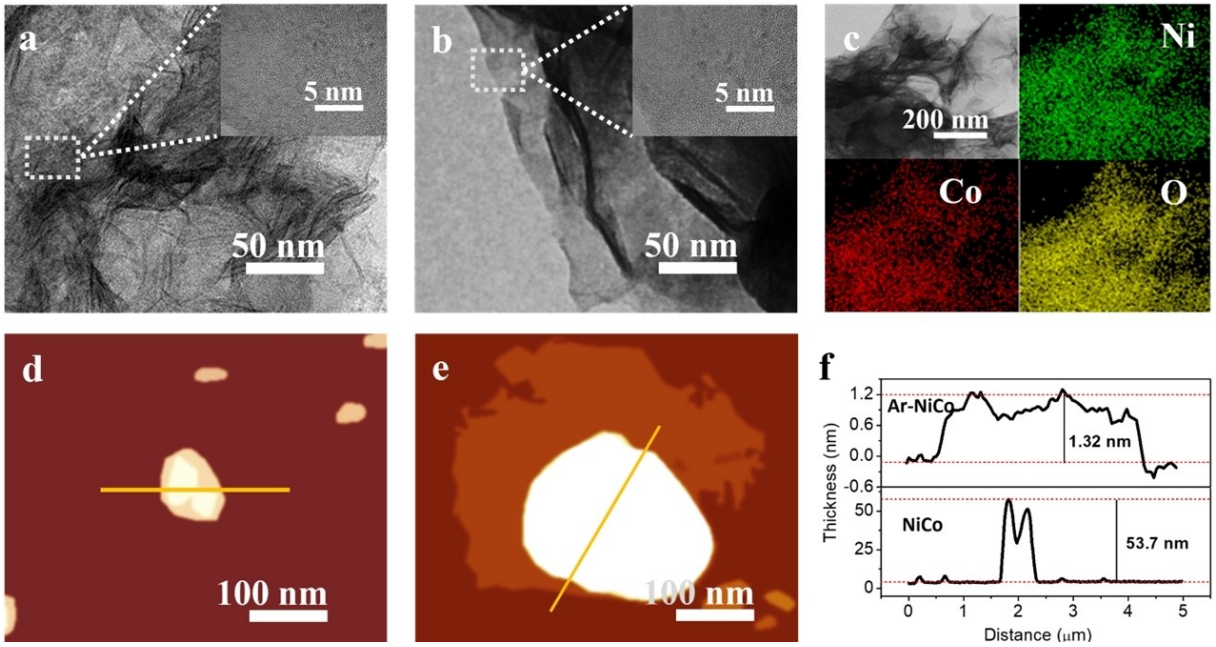

Figure 2. Electron microscopic characterization of Ar-NiCoO$_x$ nanosheets. TEM (inset: HRTEM) for a) NiCoO$_x$, b) Ar-NiCoO$_x$, c) EDX mapping images of Ar-NiCoO$_x$, AFM images of d) NiCoO$_x$, e) Ar-NiCoO$_x$, and f) corresponding height curves.

100 mA cm^{-2}. Figure 4(c) shows comparison of GCD curves of Ar-NiCoO$_x$, NiCoO$_x$, and NF electrode materials. Under the same current density and potential window, the discharge of Ar-NiCoO$_x$ electrode is longer and acquired wider potential plateau than those of NiCoO$_x$, and NF electrode materials, manifesting good reversibility and high capacitance. Figure 4(d) shows GCD curves of ultrathin Ar-NiCoO$_x$ nanosheets recorded by varying current densities.

Potential-time curves with symmetric features at all current densities and charge storage and release against time lapse are indicator of good reversibility, low polarization, and improvement in the Coulombic efficiency of Ar-NiCoO$_x$ nanosheets. The areal capacitance of Ar-NiCoO$_x$, NiCoO$_x$, and NF electrode materials were calculated based on charge-discharge curves from Figures 4(d) and S5(a, b), respectively, and the results are plotted against discharging current density in Figure 4(e). Encouragingly, the Ar-NiCoO$_x$ nanosheet electrode exhibits excellent areal capacitance of 5.7, 4.3, 3.0, 2.2, 1.9, 1.7, and 1.6 F cm^{-2} at current densities of 5, 10, 20, 40, 60, 80 and 100 A cm^{-2}. Compared to Ar-NiCoO$_x$ nanosheets, NiCoO$_x$ LDHs and NF demonstrated lower areal capacitance at the same current densities, indicating the effectiveness of Ar-plasma-induced exfoliation. The areal capacitance of Ar-NiCoO$_x$ nanosheets (5.7 F cm^{-2}) is almost five and three times that of NF (0.2 F cm^{-2}) and pristine NiCoO$_x$ (2.3 F cm^{-2}), respectively at a current density of 5 mA cm^{-2}. A comparison of areal capacitance of Ar-NiCoO$_x$ ultrathin nanosheet with other reported electrode materials are presented in Table S1 and the value is superior to most of the earlier reported TMLDHs electrode materials. Figure 4(f) shows the electrochemical impedance spectrum of Ar-NiCoO$_x$, NiCoO$_x$, and NF electrode materials in the frequency range of 0.01 Hz–10 kHz. Clearly, Ar-NiCoO$_x$ nanosheet demonstrated shorter diameter semicircle compared to bulk NiCoO$_x$ and NF, an indicator enhanced ion diffusion and effective electron transfer. The result infers that the superficial Ar-plasma treatment could have reduced mass transfer resistance, facilitating charge transfer kinetics across the exfoliated ultrathin nanosheets. Randles equivalent circuit is commonly used to explain the electrochemical properties of electrode-solution interfaces, including Faradic current and diffusion transport (Figure S6). A circuit consists of two parts: a high-frequency part, referred to as the electrolyte resistance (R_1), and a low-frequency part, referred to as the bulk properties. Secondly, the interface between the electrode and the film was referred to as the parallel resistance (R_2) and capacitor (C_1) of this layer, while last parallel charge transfer resistance (R_3) and double layer capacitance (C_2) describes film-solution interface.

It can also be observed that the electrochemical characteristics of Ar-NiCoO$_x$ nanosheets are also affected by the duration of the Ar-plasma treatment. The electrode material has demonstrated enhanced supercapacitive activity with increase in treatment time, where maximum activity was attained at around 20 min treatment time (Figure S7a–c). The areal capacitances of Ar-NiCoO$_x$ nanosheets with prolonged Ar-plasma treatment period of 20 minutes can reach as high as 5.7 F cm^{-2} (Figure 5a). Furthermore, the long-term charge/discharge performance of NiCoO$_x$ and Ar-NiCoO$_x$ nanosheets were tested at a current density of 100 mA cm^{-2} (Figure 5b). After 5000 cycles, NiCoO$_x$, and Ar-NiCoO$_x$ nanosheets maintained 84%, and 88% of their initial capacitance, respectively, indicator of good electrochemical stability. Benefiting from ultrathin and highly disordered nanostructures, and enlarged space between jammed layers, Ar-NiCoO$_x$ was characterized by

Research Article
doi.org/10.1002/batt.202200270
Chemistry Europe
European Chemical Societies Publishing

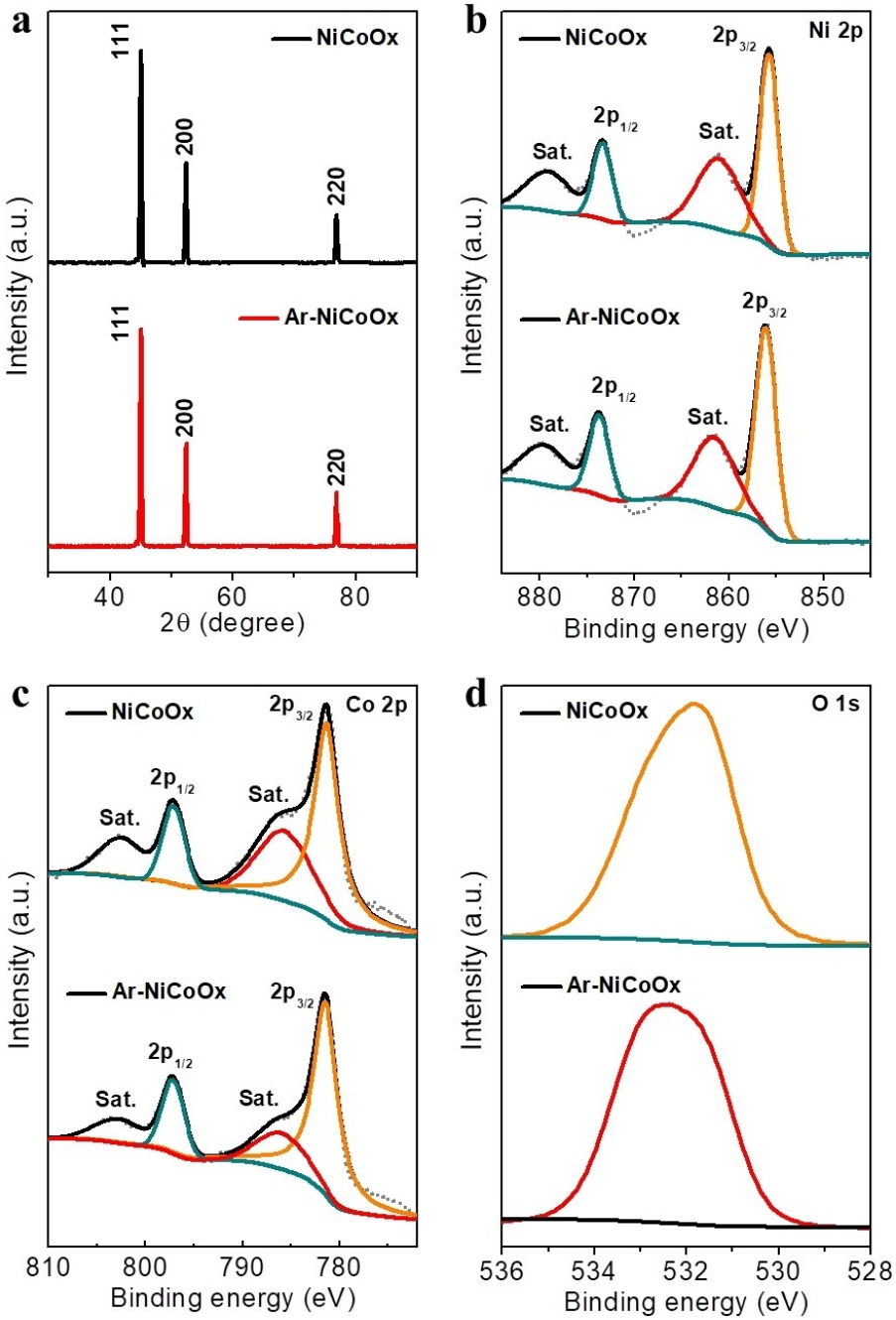

Figure 3. Spectroscopic characterization of Ar-NiCoO$_x$ nanosheets. a) XRD patterns of Ar-NiCoO$_x$, b–d) high-resolution XPS spectra of NiCoO$_x$ and Ar-NiCoO$_x$ nanosheets.

high surface area, enhanced conductivity, fast charge transfer kinetics, and superior electrochemical stability.

To further estimate the practical application of Ar-NiCoO$_x$ nanosheets, symmetric supercapacitor was constructed by coupling Ar-NiCoO$_x$ nanosheets as positive electrode and negative electrodes. As shown in the Figure S8(a), the cyclic voltammograms almost keep their quasi-rectangular shape with the increasing scan rate, confirming the perfect capacitive performance and rapid current response of the symmetric supercapacitor. The GCD curves at various current densities within potential window of 0–1.6 V suggest an efficient charge-discharge reversible response (Figures S8b). The material also exhibited excellent capacitance retention of 80% after 1500 cycles (Figures S8c). Figure S8(d) shows the Ragone diagram of the device, which shows that an energy density of 85.9 μWh cm^{-2} was measured at a power density of 500 μW cm^{-2}. Compared with the previous work, the performance of our electrode material is better, indicating that the device has a broader application prospect.[30–33]

Research Article
doi.org/10.1002/batt.202200270
Chemistry Europe
European Chemical Societies Publishing

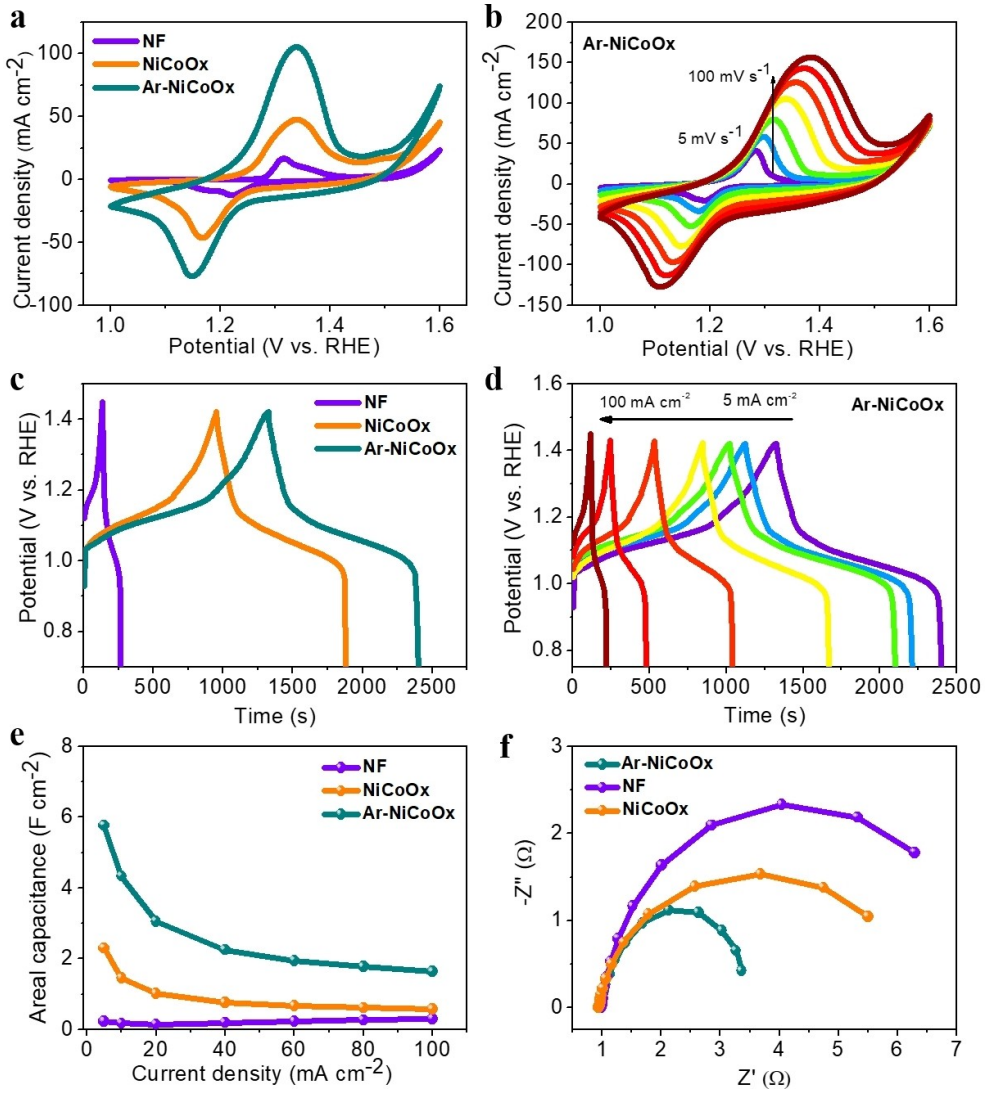

Figure 4. Electrochemical characterization of Ar-NiCoO$_x$ nanosheets in the positive potential range. a) Comparison of the CV profiles of NF, NiCoO$_x$, and Ar-NiCoO$_x$; b) CV profiles of Ar-NiCoO$_x$ at different scan rates; c) Comparison of GCD profiles of NF, NiCoO$_x$, and Ar-NiCoO$_x$ at 5 mA cm^{-2}; d) GCD profiles of Ar-NiCoO$_x$ nanosheets at different current densities; e) Areal capacitance estimated from GCD; f) EIS Nyquist plots.

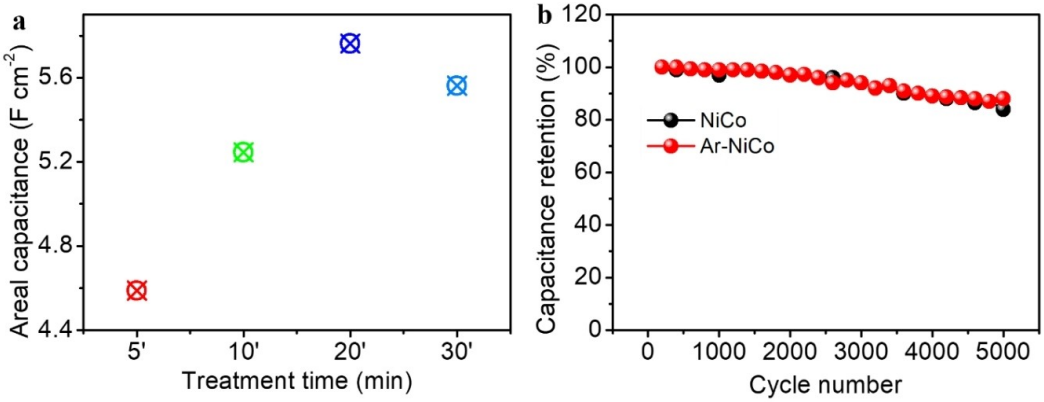

Figure 5. Electrochemical performance. a) Areal capacitance of Ar-NiCoO$_x$ nanosheets at different Ar-plasma treatment times obtained at a current density of 5 mA cm^{-2}; b) Cycling stability of NiCoO$_x$ and Ar-NiCoO$_x$ nanosheets.

Conclusion

In summary, we have demonstrated an effective and environmentally friendly strategy to exfoliate bulk LDHs into ultrathin nanosheets. By using superficial non-thermal Ar-plasma exfoliation technique, we were able to fabricate a single layer of nanosheets from pristine $NiCoO_x$ LDHs. As a result, the electrode material Ar-$NiCoO_x$ (5.7 F cm^{-2}) exhibited an areal capacitance almost three times that of pristine $NiCoO_x$ (2.3 F cm^{-2}) at current density of 5 A cm^{-2} and excellent cycling stability with over 88% capacitance retention after 5000 cycles. Such high-capacity density and cycle stability is mainly attributed to increased surface area and improved charge transport induced by Ar-plasma exfoliation of the pristine LDHs. The concept proposed in this work may open opportunities to tune the structural and electrochemical properties of TMLDHs for their use as high-energy supercapacitors.

Experimental Section

Material synthesis

The NiCo-LDHs nanosheet was synthesized using electrodeposition method on nickel foam. The electrodeposition was carried using a standard three-electrode system from a solution containing Ni-$(NiO_3)_2.6H_2O$ and $Co(NO_3)_2.6H_2O$ salts at −1.0 V vs. Ag/AgCl for 400 s. Once the deposition was completed, the material was rinsed with DI water and left to dry in air. Finally, the dried sample was treated using non-thermal Ar-plasma of 100 W polarization for a defined period.

Characterization

SEM and TEM images were taken using FE-SEM S-4700, Hitachi, and TEM, JEM-2100F, JEOL Ltd., Tokyo, Japan, respectively. Material composition and surface electronic characterization were done using XPS with K-α XPS (Themo Scientific), XRD data was obtained by Empyrean series 2; PANalytical, Netherlands, and AFM (Veeco dilnnova, USA). Electrochemical characterization was performed using an Iviumstat (Eindhoven, Netherlands) workstation where Ar-NiCo, NiCo, and NF (1 cm^2 in area) are directly used as the working electrode, platinum wire and Ag/AgCl (3 M KOH) are used as a counter electrode and reference electrode, respectively. Cyclic voltammetry (CV) and galvanostatic charge-discharge (GCD) tests were carried out using three-electrode configuration. The CV curves were measured in a potential range between 0.0 and 0.6 V at different scan rates, and the GCD were measured within potential of −0.1 to 0.45 V at different current densities in 3 M KOH electrolyte. The cyclic stability was evaluated by CV measurements at a current density of 100 mA cm^{-2} for over 5000 cycles. The areal capacitance (F cm^{-2}) of the electrode was calculated using equation $C = \frac{Jt}{\Delta V}$, where J is the current density (A cm^{-2}), t is the discharge time (s), and $\triangle V$ (V) is the potential window for the cycling test.

To evaluate the practical application of the as synthesized electrode material, an asymmetric supercapacitor device was assembled by using Ar-$NiCoO_x$/NF as positive electrode and rGO/NF as a negative electrode. The device was characterized in 3 M KOH electrolyte and filter paper was employed as the separator to prevent the short circuit between the two electrodes.

Acknowledgements

This work was supported by National Research Foundation of Korea (NRF-2021H1D3A2A01099457, 2021K1A3A1A16096990, 2019R1A2C2007825).

Conflict of Interest

The authors declare no conflict of interest.

Data Availability Statement

The data that support the findings of this study are available from the corresponding author upon reasonable request.

Keywords: Ar-plasma exfoliation · high stability · nanosheet · $NiCoO_x$ LDHs · supercapacitor

[1] B. B. Gicha, L. T. Tufa, Y. Choi, J. Lee, *ACS Appl. Energ. Mater.* **2021**, *4*, 6833–6841.
[2] L. T. Tufa, B. B. Gicha, H. Wu, J. Lee, *Batteries & Supercaps* **2020**, *4*, 429–444.
[3] W. Jiang, D. Yu, Q. Zhang, K. Goh, L. Wei, Y. Yong, R. Jiang, J. Wei, Y. Chen, *Adv. Funct. Mater.* **2015**, *25*, 1063–1073.
[4] K. Saravanan, C. W. Mason, A. Rudola, K. H. Wong, P. Balaya, *Adv. Energy Mater.* **2013**, *3*, 444–450.
[5] Y. Liao, H. Wang, M. Zhu, A. Thomas, *Adv. Mater.* **2018**, *30*, 1705710.
[6] N. Wu, X. Bai, D. Pan, B. Dong, R. Wei, N. Naik, R. R. Patil, Z. Guo, *Adv. Mater. Interfaces* **2021**,*8*, 2001710.
[7] M.-Q. Zhao, Q. Zhang, J.-Q. Huang, F. Wei, *Adv. Funct. Mater.* **2012**, *22*, 675–694.
[8] L. Lv, Z. Yang, K. Chen, C. Wang, Y. Xiong, *Adv. Energy Mater.* **2019**, *9*, 1803358.
[9] Y. Wang, Y. Liu, Z. Chen, M. Zhang, B. Liu, Z. Xu, K. Yan, *Green Chem. Eng.* **2022**, *3*, 53–63.
[10] Y. Wang, Z. Chen, M. Zhang, Y. Liu, H. Luo, K. Yan, *Green Chem. Eng.* **2022**, *7*, 1053–1061.
[11] X. Gao, P. Wang, Z. Pan, J. P. Claverie, J. Wang, *ChemSusChem* **2020**, *13*, 1226–1254.
[12] B. B. Gicha, L. T. Tufa, S. Kang, M. Goddati, E. T. Bekele, J. Lee, *Nanomaterials* **2021**,*11*, 1388.
[13] H. Yi, S. Liu, C. Lai, G. Zeng, M. Li, X. Liu, B. Li, X. Huo, L. Qin, L. Li, M. Zhang, Y. Fu, Z. An, L. Chen, *Adv. Energy Mater.* **2021**, *11*, 2002863.
[14] Y. Wang, D. Yan, S. El Hankari, Y. Zou, S. Wang, *Adv. Sci.* **2018**, *5*, 1800064.
[15] T. Wang, F. Yu, X. Wang, S. Xi, K.-J. Chen, H. Wang, *Electrochim. Acta* **2020**, *334*, 135586.
[16] Y. Shabangoli, M. S. Rahmanifar, A. Noori, M. F. El-Kady, R. B. Kaner, M. F. Mousavi, *ACS Nano* **2019**, *13*, 12567–12576.
[17] C. Chen, L. Tao, S. Du, W. Chen, Y. Wang, Y. Zou, S. Wang, *Adv. Funct. Mater.* **2020**, *30*, 1909832.
[18] W. Quan, C. Jiang, S. Wang, Y. Li, Z. Zhang, Z. Tang, F. Favier, *Electrochim. Acta* **2017**, *247*, 1072–1079.
[19] J. Li, P. Zhang, X. Zhao, L. Chen, J. Shen, M. Li, B. Ji, L. Song, Y. Wu, D. Liu, *J. Colloid Interface Sci.* **2019**, *549*, 236–245.
[20] Y. Wang, Y. Zhang, Z. Liu, C. Xie, S. Feng, D. Liu, M. Shao, S. Wang, *Angew. Chem. Int. Ed.* **2017**, *56*, 5867–5871; *Angew. Chem.* **2017**, *129*, 5961–5965.
[21] H. Liang, F. Ming, H. N. Alshareef, *Adv. Energy Mater.* **2018**, *8*, 1870126.
[22] C. Yuan, J. Li, L. Hou, X. Zhang, L. Shen, X. W. Lou, *Adv. Funct. Mater.* **2012**, *22*, 4592–4597.
[23] H. He, J. Lian, C. Chen, Q. Xiong, M. Zhang, *Chem. Eng. J.* **2021**, *421*, 129786.
[24] X. Lu, C. Zhao, *Nat. Commun.* **2015**, *6*, 6616.

[25] M. C. Biesinger, B. P. Payne, A. P. Grosvenor, L. W. M. Lau, A. R. Gerson, R. S. C. Smart, *Appl. Surf. Sci.* **2011**, *257*, 2717–2730.
[26] R. Liu, Y. Wang, D. Liu, Y. Zou, S. Wang, *Adv. Mater.* **2017**, *29*, 1701546.
[27] M. C. Biesinger, B. P. Payne, L. W. M. Lau, A. Gerson, R. S. C. Smart, *Surf. Interface Anal.* **2009**, *41*, 324–332.
[28] H. Wang, Q. Gao, L. Jiang, *Small* **2011**, *7*, 2454–2459.
[29] L. T. Tufa, S. Oh, J. Kim, K.-J. Jeong, T. J. Park, H.-J. Kim, J. Lee, *Electrochim. Acta* **2018**, *290*, 369–377.
[30] L. Zhang, H. Xia, S. Liu, Y. Zhou, Y. Zhao, W. Xie, *Nanoscale Res. Lett.* **20217**, *16*, 83.
[31] Y. Chen, B. Xu, J. Wen, J. Gong, T. Hua, C. W. Kan, J. Deng, *Small* **2018**, *14*, 1704373.
[32] M. Ojha, M. Deepa, *Chem. Eng. Sci.* **2019**, *368*, 772–783.
[33] S. C. Sekhar, G. Nagaraju, J. S. Yu, *Nano Energy* **2017**, *36*, 58–67.

Manuscript received: June 16, 2022
Revised manuscript received: August 23, 2022
Accepted manuscript online: August 25, 2022
Version of record online: September 19, 2022